OPEN

Enhanced Surface Properties of Light-Trapping Si Nanowires Using Synergetic Effects of Metal-Assisted and Anisotropic Chemical Etchings

Youngsoon Jeong[1], Chanwoo Hong[1], Yeong Hun Jung[1], Rashida Akter[1], Hana Yoon[2] & Ilsun Yoon[1]*

Metal-assisted chemical etching (MACE) has been widely explored for developing silicon (Si)-based energy and optical devices with its benefits for low-cost and large-area fabrication of Si nanostructures of high aspect ratios. Surface structures and properties of Si nanostructures fabricated through MACE are significantly affected by experimental and environmental conditions of etchings. Herein, we showed that surfaces and interfacial energy states of fabricated Si nanowires can be critically affected by oxidants of MACE etching solutions. Surfaces of fabricated Si nanowires are porous and their tips are fully covered with lots of Si nano-sized grains. Strongly increased photoluminescence (PL) intensities, compared to that of the crystalline Si substrate, are observed for MACE-fabricated Si nanowires due to interfacial energy states of Si and SiO$_x$ of Si nano-sized grains. These Si grains can be completely removed from the nanowires by an additional etching process of the anisotropic chemical etching (ACE) of Si to taper the nanowires and enhance light trapping of the nanowires. Compared with the MACE-fabricated Si nanowires, ACE-fabricated tapered Si nanowires have similar Raman and PL spectra to those of the crystalline Si substrate, indicating the successful removal of Si grains from the nanowire surfaces by the ACE process.

Silicon (Si) nanowires have been extensively studied due to their unique properties and great potentials in applications for optical and electrical sensors and energy conversion and storage devices[1–4]. Simple and large-area fabrications of vertically aligned Si nanowires have been widely developed for efficient and cost-effective Si photovoltaics due to their benefits of efficient light trapping and short carrier collection paths[5–7]. Metal-assisted chemical etching (MACE), in which Si is vertically etched in a mixed solution of HF and H$_2$O$_2$ with a patterned catalyst of noble metals (e.g., Ag and Au), has attracted significant interest as a simple and cost-effective etching method for fabricating vertically aligned Si nanowires[8–10].

MACE is based on simple redox reactions those occur on the interfaces of catalytic metals and a Si substrate[1,2,11–13]. Holes (h$^+$), created by the reduction of H$_2$O$_2$ on the metal surface, are transferred to the underlying Si substrate and oxidize the Si atoms of the substrate as schemed in Fig. 1(a)[2,11–13]. These oxidized Si atoms are then etched by HF in the etching solution. The underlying Si substrate can be vertically etched as MACE of the Si substrate is proceeded continuously.

In the fabrication of vertically aligned Si nanowires through MACE, the length of nanowires are usually controlled with the reaction time and the diameter and interspace of the nanowires are controlled with the patterned structure of catalytic metals, respectively[14,15]. The reaction rates of MACE and the structures of Si nanowires can be critically affected by the reaction conditions including materials and surface structures of catalytic metals, reaction temperatures, compositions of the etching solution, crystallographic orientations, and types and concentrations of dopants of the Si substrate[1,11,16,17]. In MACE, the holes transferred to the Si substrate are mainly used up for the oxidization of Si atoms near the catalytic metals[10,15,18,19]. However, these holes can result in additional

[1]Department of Chemistry, Chungnam National University, Daejeon, 34134, Republic of Korea. [2]Korea Institute of Energy Research (KIER), Daejeon, 34129, Republic of Korea. *email: ilsunyoon@cnu.ac.kr
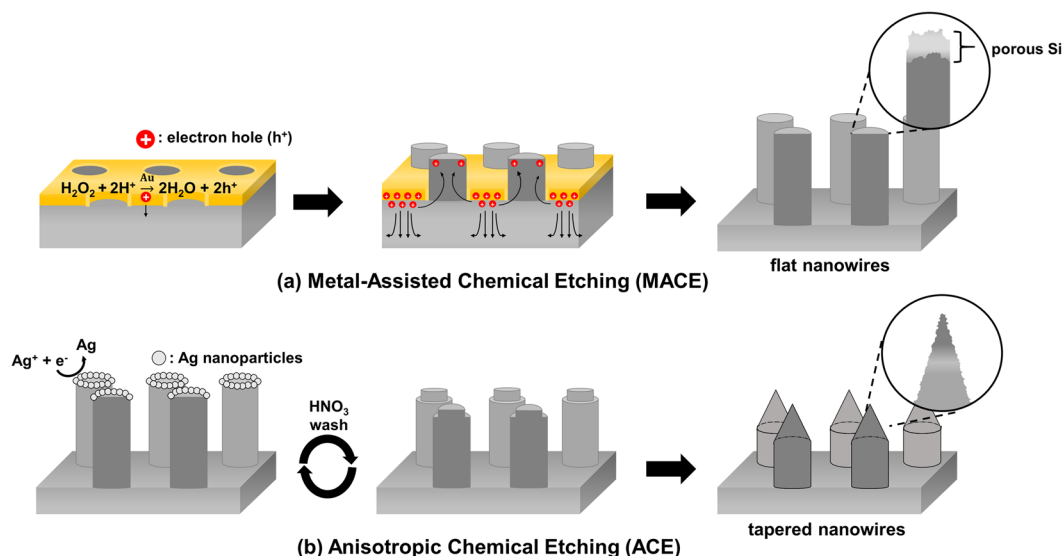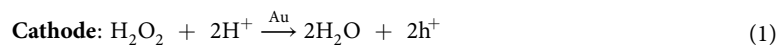
Figure 1. Schematic of the fabrication processes of vertically etched flat and tapered Si nanowires. (**a**) Si nanowires are vertically etched by MACE of a Si (100) substrate. The holes, generated excessively on the interface of the Au mask and the Si substrate during the MACE process, can be diffused and accumulated in the Si substrate and Si nanowires. These accumulated holes can make the nanowire surfaces oxidized and porous with Si nano-sized grains during and after the MACE process. (**b**) Unstable Si atoms and Si grains can be effectively removed from the nanowire surface by performing multiple rounds of ACE, which etches the nanowires selectively to obtain tapered shapes.

oxidations and etchings of the surface and interior of the Si nanowires and substrates if excess holes are created on the catalytic metals and diffused into the Si substrate and nanowires[2,11,16]. Since the oxidant concentration in the etching solution is critical for hole generations on the catalytic metal surface, surface structures and morphologies of fabricated Si nanowires can be significantly affected by the concentration of H_2O_2 in the etching solution[1,13,20]. By this reason, the concentration of H_2O_2 needs to be optimized for fabricating Si nanowires through MACE.

In this study, we investigate the influences of H_2O_2 on Si nanowire surfaces and on their interfacial energy states during the MACE process with electron microscopy, and Raman and photoluminescence (PL) spectroscopy studies. Surfaces of MACE-fabricated Si nanowires are highly porous and their tips are covered with lots of Si nano-sized grains which could be easily oxidized during and after the MACE process. The formation and oxidization of the Si nano-sized grains on the nanowire surfaces are strongly affected by etching procedures and conditions[8,18,20–22], contributing in significant increases in PL intensities of the nanowires[9,17]. These Si nano-sized grains and their interfaces can be completely removed from the nanowire surface by selective etching of reactive Si atoms with the anisotropic chemical etching (ACE). The Si nanowires are vertically tapered during the ACE processes, to afford sharp tip ends, significantly enhanced light trapping and highly suppressed PL emission[5,6,8,21–23]. To better understand how surface oxidation of the Si nanowires during the MACE process will affect on crystallinities and interfacial energy states of the tapered Si nanowires of the ACE process, which is the post-etching process of the MACE process, changes in surface morphologies and optical properties of the tapered nanowires are compared with those of the MACE fabricated nanowires.

Results and Discussion
The MACE mechanism is generally considered to involve several redox reactions near the catalytic metal surface including H_2O_2 reduction in the etching solution on the catalyst surface (Eq. 1), injection of holes into the underlying Si substrate, oxidation of Si atoms due to the injected holes (Eq. 2) and etching of the oxidized Si atoms by HF[1,11]. The half reactions of reduction and oxidation involved in MACE with Au catalysts can be described as follows[9,23,24]:

$$\textbf{Cathode}: H_2O_2 \ + \ 2H^+ \ \xrightarrow{Au} \ 2H_2O \ + \ 2h^+ \tag{1}$$

$$\textbf{Anode}: Si \ + \ 6HF \ + \ 4h^+ \ \rightarrow \ SiF_6^- \ + \ 6H^+ \tag{2}$$

As described in Fig. 1(a), the holes injected into the underlying Si substrate are mainly consumed by oxidization of Si atoms near the catalytic Au. These oxidized Si atoms are etched by HF in the etching solution. These redox reactions proceed continuously on the Si substrate with the patterned Au catalyst and vertically etched Si nanowires of high aspect ratio are formed by MACE. Although there might be differences depending on the type and concentration of dopants of the Si substrate, holes excessively produced and injected into the Si substrate can be diffused and accumulated in the interior of the substrate or along the nanowires. These excess holes can
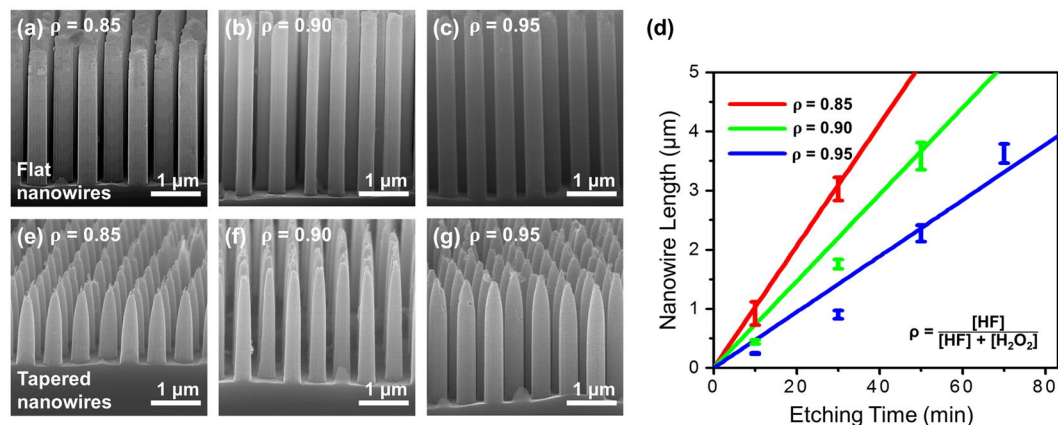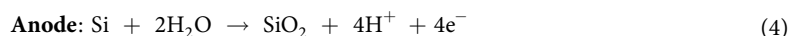
Figure 2. SEM images of vertically etched flat and tapered Si nanowires. Flat nanowires are fabricated in MACE etching solutions of different HF compositions ($\rho = [HF]/([HF] + [H_2O_2])$) of (**a**) 0.85, (**b**) 0.90 and (**c**) 0.95. (**d**) The reaction time is controlled from 30 min to 70 min for each MACE process to obtain Si nanowires with similar lengths of 3 μm. (**e–g**) Flat Si nanowires of different ρ values are anisotropically etched to taper the tip ends of nanowires.

contribute to additional etchings of the structures and could increase the surface porosity of the nanowires with Si nano-sized grain formation, as described in Fig. 1(b)[2,12,13].

As mentioned in the introduction, the structures of the MACE-fabricated Si nanowires can be affected by several experimental factors such as temperature, humidity, materials and structures of catalysts, and composition of the etching solution[1,11,14]. The rates of reduction reaction on the Au surface and the hole injection into the Si substrate are critically increased with the oxidant concentration in the MACE process. Surface morphologies and interfacial energy states of the etched Si nanowires are significantly affected by the H_2O_2 concentration in the etching solution.

In this study, Si nanowires are fabricated in etching solutions with different HF compositions (ρ, $\rho = [HF]/([HF] + [H_2O_2])$) to investigate the influence of the oxidant on their morphology and structure, as shown in Fig. 2(a–c). The HF concentration is fixed at 3.5 M, while the ρ value is adjusted to 0.85, 0.90, and 0.95 for each etching solutions by controlling the H_2O_2 concentration to 0.62, 0.39, and 0.18 M, respectively. All MACE processes are proceeded in etching solutions of different ρ values and the reaction time is changed to control the length of the Si nanowire for each condition, as shown in Fig. 2(d). As the HF composition is increased and the H_2O_2 concentration is decreased in the etching solution, the hole-generation and injection into the Si substrate would be decreased during the MACE processes. As a result, the etching rate, determined from the length of the etched nanowires, is decreased to 0.1, 0.08 and 0.06 μm/min with an increase in the ρ value, respectively. In this study, the nanowires are vertically etched to obtain lengths of 3−4 μm for effective light trapping without agglomeration during drying. The reaction times are controlled within 30 to 70 min with ρ values increased from 0.85 to 0.95. Lengths of fabricated nanowires are measured as 3.0 ± 0.3, 3.6 ± 0.2, and 3.6 ± 0.2 μm for each etching conditions. As shown in Fig. 1(b), the ACE processes are performed with these MACE-fabricated Si nanowires to make the nanowires having pencil-like sharpened tip ends for their enhanced light trapping[3,6,22–24]. The ACE process involves reduction of Ag ions (Eq. 3) and oxidation and etching of Si atoms (Eqs. 4 and 5) and these redox reactions are proceeded selectively on reactive Si atoms of sharp edges or Si nano-sized grains of the nanowires[8,18,22]. Ag nanoparticles are grown on the Si nanowire surface during the reduction and completely removed from the Si surface completely in the HNO_3 solution. These multiple processes are repeated seven times, sequentially to form tapered Si nanowires as shown in Fig. 2(e–g).

$$\textbf{Cathode}: Ag^+ + e^- \rightarrow Ag \tag{3}$$

$$\textbf{Anode}: Si + 2H_2O \rightarrow SiO_2 + 4H^+ + 4e^- \tag{4}$$

$$SiO_2 + 6HF \rightarrow [SiF_6]^{2-} + 2H_2O + 2H^+ \tag{5}$$

Besides changes in the tip ends of the Si nanowires, the lengths of the nanowires are decreased in the ACE process and are measured to be 1.7 ± 0.1, 2.2 ± 0.2, and 2.7 ± 0.1 μm, with an increase in ρ values. Compared the lengths of flat and tapered Si nanowires fabricates with the MACE and ACE processes, tapered nanowires of ACE are shorter than flat nanowires of MACE, showing that length ratios of the tapered nanowires relative to the flat nanowire increase from 0.57 (ρ = 0.85) to 0.73 (ρ = 0.95) with an increase in the ρ value. This dependence can be attributed to that the nanowire surface, etched by MACE of a higher ρ value, i.e., lower H_2O_2 concentration, is stable and less oxidized during the MACE process.

As expected, due to anti-reflection enhanced by their sharpened tip structures, the surface reflection of tapered Si nanowires is measured as much lower compared to those of the flat Si nanowires, as shown in Fig. 3(a)[25,26]. Compared to the average reflectance in the wavelength region of 450–900 nm (R_{avg}) of 35% of the bulk c-Si
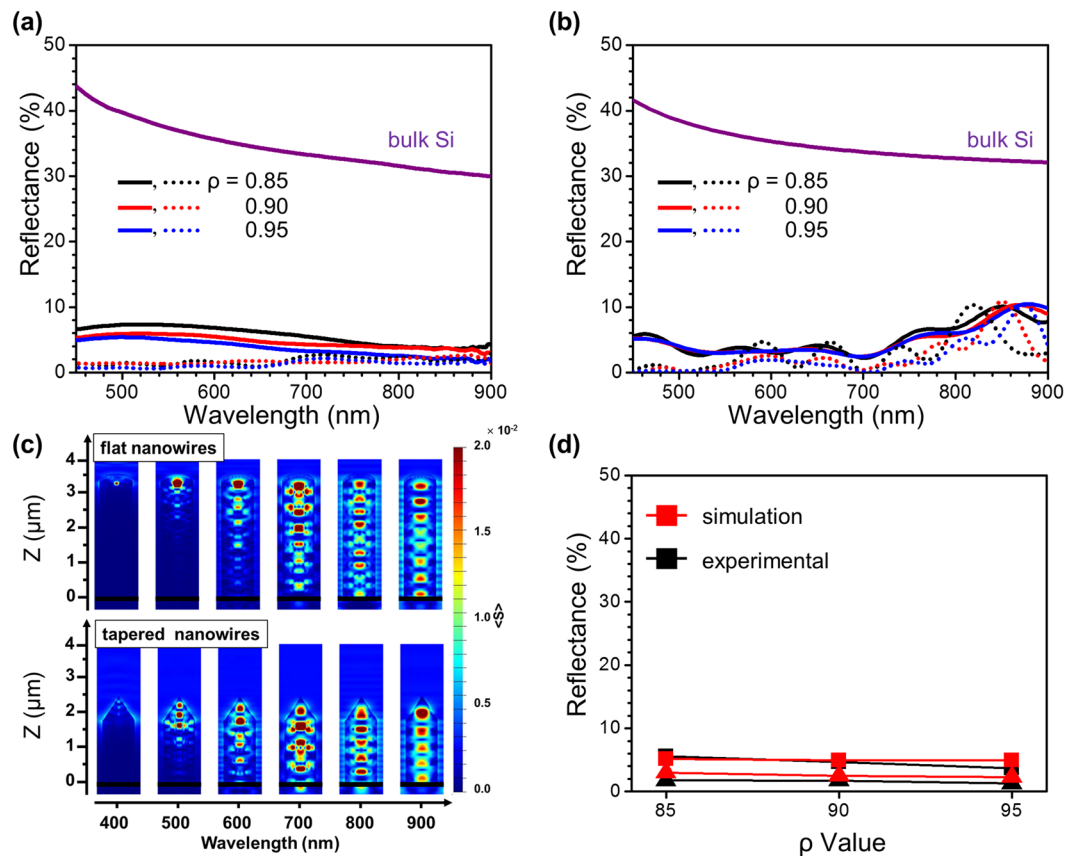
Figure 3. Comparison of (**a**) experimental and (**b**) simulated reflectances of (solid) flat and (dot) tapered Si nanowires of different etching compositions (ρ) of (black) 0.85, (red) 0.90 and (blue) 0.95 and of the (violet) bulk c-Si substrate. (**c**) Cross-sections of distribution of the time-averaged Poynting vector (<S>) near the (upper) flat and (lower) tapered nanowires of ρ = 0.95, calculated in wavelength region of 400–900 nm. (**d**) (black) Experimental and (red) simulated reflectance spectra of flat (■) and tapered (▲) nanowires of each ρ value are averaged in the wavelength range of 450–900 nm for comparison. All of simulations have been performed with a commercialized FDTD solution (Lumerical Solution, Lumerical Inc.)[41].

substrate, R_{avg} of the flat Si nanowires etched by MACE is significantly decreased to less than 7% for all nanowires. With an increase in ρ values from 0.85 to 0.95, R_{avg} of the flat nanowires decrease from 6.1% to 4.1%. The R_{avg} values of all tapered nanowires fabricated by ACE, further decrease to less than 2% showing a minimum value of 1.1% for the nanowire of ρ = 0.95. Figure 3(b) shows the reflectance spectra of flat (solid lines) and tapered (dots lines) Si nanowires simulated with the FDTD method[3,6,27,28]. The lengths of the Si nanowires considered in the simulation are used according to the SEM images of the nanowires shown in Fig. 2. MACE-fabricated flat nanowires and ACE-fabricated tapered nanowires are assumed to have roughed tip surfaces considering their TEM images shown in Fig. 5 (See the Supporting Information, Figure S1 for detail).

For further understanding of the light trapping of the Si nanowires, we investigate the cross-sections of the time-averaged Poynting vectors, <S>, near the flat and tapered nanowires of ρ of 0.95 at wavelengths ranging from 400 to 900 nm, as shown in Fig. 3(c). <S> represents the power distribution near the structures[29]. Cross-sections of power distributions near the nanowires show significant light trapping of shorter wavelength of <700 nm near the tip of the Si nanowire, indicating that the tip structure of the Si nanowire is critical for its light trapping.

Figure 3(d) shows the averaged values of the simulated (red) and experimental (black) reflectance over the entire wavelength range from 450 to 900 nm of flat (square) and tapered (triangle) Si nanowires with respect to their ρ values. As described above, the significant decrease in the surface reflection, and thus, the enhancement of light trapping of the nanowires through a change of their tip structures is confirmed. The surface reflections of Si nanowires fabricated with MACE and ACE show a slight decrease with an increase in ρ values and this slight change can be explained with increased light trappings of porous nanowires due to the surface structures in their length directions.

Figure 4(a) shows the EDS line profiles for a comparison of element distributions of O and Si in the longitudinal direction of the Si nanowires, etched by MACE of ρ = 0.95. In these EDS line profiles, the intensity of O was observed more strongly at the tip end of the nanowire than near the substrate[20,30]. The Fig. 4(b) shows a comparison of the photoluminescence (PL) spectra of flat (upper) and tapered (lower) Si nanowires of different ρ values, indicating significant dependence of PL spectra of the nanowires with characteristic PL emissions of porous Si structures near λ = 700 nm on their etching procedures and structures[31–34]. Especially, the flat and
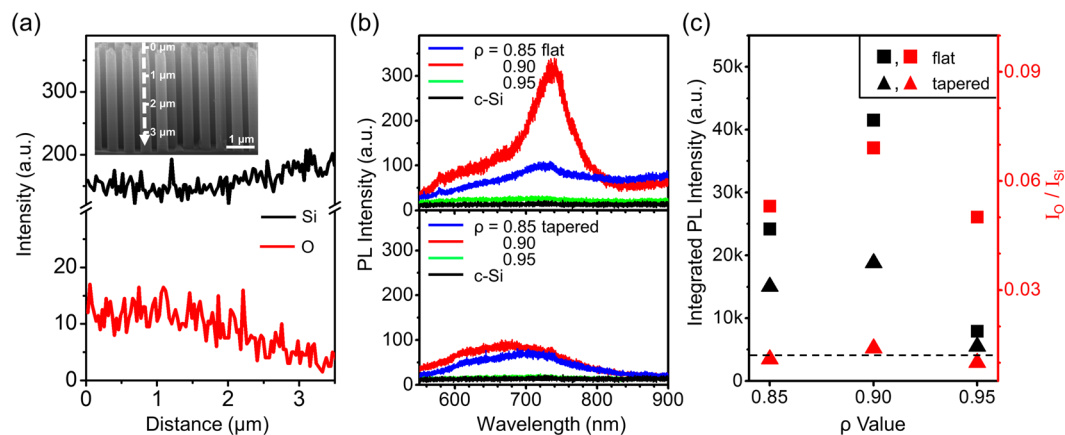
Figure 4. (**a**) EDS line profiles of Si (black) and O (red) components along the flat Si nanowire of $\rho = 0.95$, indicated as a dash line on the Si nanowire in the SEM image (inset), (**b**) PL spectra of flat (upper) and tapered (lower) Si nanowires of ρ of 0.85 (blue), 0.90 (red), and 0.95 (green) and the PL spectrum of the bulk c-Si substrate (black). (**c**) Comparison of integrated PL intensities of flat (■) and tapered (▲) nanowires at the wavelength range of 550–900 nm and ratios of integrated EDS intensities of O (I_O) and Si (I_{Si}) of flat (■) and tapered (▲) nanowires. The black dash line indicates the integrated PL intensity of the bulk c-Si substrate.
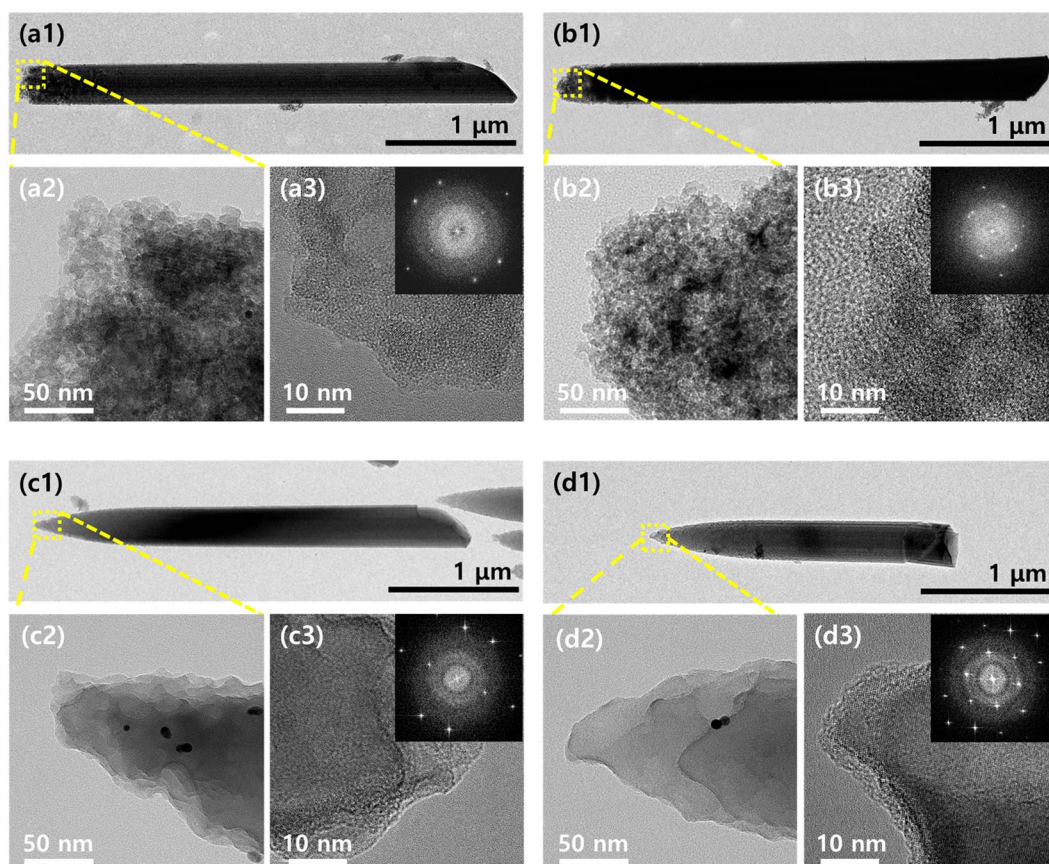

Figure 5. TEM images taken from flat Si nanowires of (a1–a3) $\rho = 0.95$ and (b1–b3) $\rho = 0.90$ and from tapered Si nanowires of (c1–c3) $\rho = 0.95$ and (d1–d3) $\rho = 0.90$, respectively. Inset figures of HRTEM images of a3, b3, c3 and d3 are diffraction patterns achieved by using the fast Fourier transform (FFT) of the HRTEM images to compare crystallinities of the flat and tapered Si nanowires.

tapered nanowires of $\rho = 0.95$ are observed to exhibit lower PL intensities, similarly to the PL intensity of the bulk c-Si substrate. These EDS line profiles (red) and PL spectra (black) of the flat (■) and tapered (▲) Si nanowires are compared in Fig. 4(c). To compare the O and Si compositions of the flat and tapered Si nanowires fabricated

under MACE conditions with different ρ values, EDS line profiles of O and Si were measured from five different nanowires. Ratios of integrated EDS intensities along the nanowires of O (I_O) and Si (I_{Si}) were averaged and compared in the Fig. 4(c). The PL spectra taken from the flat and tapered nanowires are integrated over all wavelength regions, and their integration values are compared in Fig. 4(c) as well.

As described above, hole generations on catalytic Au surfaces during MACE are strongly influenced by H_2O_2 concentration in the etching solution and the excess holes injected into the Si substrate are diffused into the substrate and on the nanowires, causing secondary etchings of the structures. In particular, holes diffused into the nanowires are accumulated at their tip end, such that the tip ends become more porous with lots of Si nano-sized grains which can be easily oxidized during and after MACE due to their higher surface energies. Therefore, I_O/I_{Si} values are observed to be relatively higher on the nanowires etched in etching solutions of lower ρ values, where holes are excessively generated during MACE. Si atoms and grains of higher surface energies can be effectively removed from the nanowires by ACE, showing about ~20% decreases of I_O/I_{Si} values for the tapered nanowires compared to those of the flat nanowires.

Porous Si nanowires covered with Si nano-sized grains have various energy states available due to the formation of Si/SiO$_x$ interfaces and the quantum confinement effect of Si nanocrystals[9,18,20]. Theses defect energy states significantly increase the electron-hole recombination rates and PL emissions of the Si nanowires. Similarly to the EDS analysis, integrations of PL intensities show significant decrease when the nanowires are fabricated in the etching solutions of ρ = 0.95, where the hole injection into the Si substrate and the surface oxidation of the nanowires are minimized. PL intensities of tapered nanowires fabricated with ACE are decreased to 50% as compared to those of the MACE-fabricated flat nanowires. The tapered nanowires of ρ = 0.95 show lowest PL intensities, which are comparable to that of the bulk c-Si substrate (black dash line), indicating that unstable Si atoms and nano-sized grains formed on the Si nanowires are almost removed during the ACE process.

Figure 5 shows transmission electron microscope (TEM) images of flat (a1−a3) and (b1−b3) and tapered (c1−c3) and (d1−d3) Si nanowires of ρ = 0.95 and 0.90, respectively. The Si nanowires are carefully transferred from their substrates onto the TEM grid. TEM images of Fig. 5 (a2) and (b2) show that MACE-fabricated flat Si nanowires have very porous surfaces on their tip ends which are fully covered with lots of Si nano-sized grains, in contrast to middle sides of the nanowires, clearly showing the influence of oxidations occurred during MACE by holes excessively accumulated on tip ends of the nanowires[35–38]. These Si nano-sized grains formed on the nanowire surface can be completely removed during ACE, where Si atoms with higher surface energies could be selectively etched as shown in the TEM images of the tapered nanowires in Fig. 5 (c2−c3) and (d2−d3). The crystalline-structures of the flat and tapered Si nanowires are compared with high-resolution TEM (HRTEM) images taken on the tip ends of each nanowires, as shown in Fig. 5 (a3), (b3), (c3) and (d3). Inset figures show diffraction patterns achieved by using the fast Fourier transform (FFT) of the HRTEM images, indicating that surface of the tapered Si nanowires have higher crystalline qualities than those of the flat Si nanowires.

Raman analysis of fabricated Si nanowires of Figure S2 were performed to support our TEM observations that MACE-fabricated Si nanowires have porous tip surfaces covered with lots of nano-sized Si grains and these grains can be effectively removed from the nanowires by the ACE process. As shown by Figure S2(a), contributions of amorphous Si and SiO$_2$, which have characteristic broad Raman peaks below 500 cm^{-1}, are negligible in Raman spectra of fabricated Si nanowires compared to contributions of c-Si and Si nanocrystals[33,34]. We assumed that phonon modes of nano-sized Si grains can be described with phonon modes of Si nanocrystals, which have phonon modes at lower energy regions compared to the bulk c-Si (centered at 520.7 cm^{-1}) due to their phonon locations[20,38,39]. The size and composition of Si nanocrystals of fabricated Si nanowires of ρ = 0.90 and 0.95 were analyzed with fitting analysis, considering shifts to lower energies and broadenings of Raman peaks as shown in Figure S2(b,c)[20,30]. (see description for Figure S2 in Supporting Information) The comparison in Figure S2 (c) indicates significant decrease in the composition of Si nanocrystals in the nanowires fabricated by the MACE processes with the increase in ρ values and by the ACE processes.

Conclusions

In summary, we fabricated vertically aligned flat and tapered Si nanowires through chemical wet etchings of the MACE and ACE processes and investigated the influences of oxidants in the MACE etching solutions on surface structures, morphologies and interfacial energy states of fabricated Si nanowires. We showed that the Si nanowire surfaces are significantly affected by the concentration of H_2O_2 in the etching solution, which causes excessive injections of holes into the Si nanowires in its higher concentration, increasing the surface porosities of the nanowires with lots of Si nano-sized grains formed on the nanowire surfaces. These porous Si nanowires can be easily oxidized during and after the MACE process and their interfacial energy states are strongly affected by surface structure and oxidation of the nanowires, showing significant changes in the PL spectra with MACE etching conditions. The surface of these porous Si nanowires can be completely cleaned by ACE, which selectively removes unstable Si atoms from the nanowire surface. Flat Si nanowires could be engineered for tapered Si nanowires where Si grains are completely removed from the nanowire surface by the ACE process, showing enhanced light trapping as well as significant suppression of PL intensities. Our study can indicate that the surface oxidation which Si nanowires have during the MACE process can be critical in the surface crystallinities and interfacial energy states of the tapered Si nanowires of the post-MACE etching process. We believe that our study of enhancing surface properties including structural morphologies, crystallinities and interfacial energy states of Si nanowires with the MACE and ACE processes would contribute to the application and fabrication of Si nanowires for efficient Si-based energy harvesting and catalysis.

Method

Fabrication of vertically aligned Si nanostructure array. In this study, p-type (boron)-doped Si substrates (100) with the resistivity of 1–10 Ω·cm and thickness of 550 μm were used to fabricate vertically etched Si nanowires through MACE. Si substrates were cut into 1.5 × 1.5 cm² samples and treated with a pure piranha (H_2SO_4:H_2O_2 = 3:1 v/v) solution and O_2 plasma to remove impurities remaining on the substrates. Close-packed monolayers of polystyrene (PS) beads of 500 nm diameter (Thermo-Scientific, Inc.) were transferred on pre-cleaned Si substrates by the nanosphere lithography method and the size of PS beads was reduced to 350 nm by the inductively coupled plasma reactive ion etch (ICP-RIE)[40]. Au of 30 nm thickness was deposited on these substrates by using the E-beam evaporator at the deposition rate of 3 Å/s and the substrates were stored in a vacuum desiccator prior to the MACE process.

MACE of the prepared substrates were performed in an etching solution of HF (J. T. Baker, Inc.), H_2O_2 (J. T. Baker, Inc.) and deionized water for the fabrication of vertically etched Si nanowires. The concentration of HF was fixed at 3.5 M, the concentration of H_2O_2 was changed to control the composition of oxidants and ρ values (ρ = [HF]/([HF] + [H_2O_2])) were ranged between 0.85 and 0.95 for the etching solutions. All reactions described in this study were performed in the ice bath of 8 °C to minimize the formation of Si nanocrystals and the surface oxidization of the nanowires during the MACE process. The lengths of the Si nanowires were controlled using the reaction time. Remained PS beads and Au were removed from the substrate by rinsing in chlorobenzene and the diluted *aqua regia* (HCl:HNO$_3$ = 3:1 v/v) solution, respectively. The ACE process to taper MACE-fabricated Si nanowires was then performed by repeating processes of reducing AgNO$_3$ to Ag nanoparticles on tip ends of the nanowires in the mixed solution of HF and AgNO$_3$ and removing reduced Ag nanoparticles from the nanowire surfaces in the diluted HNO$_3$ solution. For each cycle of the ACE process, the concentration of HF in the HF and AgNO$_3$ solution was fixed to 2.0 M while that of AgNO$_3$ was increased by 0.1 mM from 0.4 to 1.0 mM for each cycle[8,22].

Characterization. The structures and surface morphologies of vertically etched Si nanowires were characterized during MACE and ACE processes by using the scanning electron microscope (SEM, Hitachi S-4800) and the transmission electron microscope (TEM, Tecnai G2 F30). The Raman and PL spectra of the Si nanowires were measured by using the microscope system (a high resolution Raman/PL spectrophotometer, Horiba LabRAM HR-800) with a 100 × objective (NA = 0.9). The Ar ion laser of λ = 514 nm and ~25 μW was used for PL and Raman studies of the nanowires. The PL spectra of the nanowires were measured in the wavelength region of 550–900 nm and Raman spectra of the nanowires were measured in the wavenumber region of 480–560 cm⁻¹. Reflectance of the nanowires were measured in the wavelength region of 450–900 nm.

Finite-difference time-domain simulation. The simulations were performed using the commercial finite-difference time-domain (FDTD) software package of Lumerical Solution 8.15[41]. The shapes and structures of flat and tapered Si nanowires used in the simulation were estimated from SEM images. All nanowires in the simulations were assumed to have a diameter of 350 nm and a pitch of 500 nm. The lengths of the flat nanowires (the tapered ones) were set as 3.0 (1.7), 3.6 (2.2) and 3.6 (2.7) μm, similarly to the lengths of the nanowires estimated from their SEM images. The reflectance spectra and time-averaged Poynting vector distribution of the nanowires, <S>, were simulated in the range of 400–900 nm. All simulations were performed with perfectly matched boundary conditions on the z-axis and with symmetric and anti-symmetric boundary conditions in the x- and y-directions. Simulated reflectance spectra of MACE-fabricated Si nanowires were treated with the low-pass filter to reduce large fluctuations in spectra which result from overestimated interferences between periodically spaced Si nanowires and coherent simulation light source[42,43]. The refractive index values of n and k of Si taken from the literature were considered in the simulation[44].

References

1. Huang, Z. *et al.* Metal-Assisted Chemical Etching of Silicon: A Review. *Adv. Mater.* **23**, 285–308, https://doi.org/10.1002/adma.201001784 (2011).
2. Li, L., Zhao, X. & Wong, C. P. Deep Etching of Single- and Polycrystalline Silicon with High Speed, High Aspect Ratio, High Uniformity, and 3D Complexity by Electric Bias-Attenuated Metal-Assisted Chemical Etching (EMaCE). *ACS Appl. Mater. Interfaces* **6**, 16782–16791, https://doi.org/10.1021/am504046b (2014).
3. He, J. *et al.* Enhanced Electro-Optical Properties of Nanocone/ Nanopillar Dual-Structured Arrays for Ultrathin Silicon/ Organic Hybrid Solar Cell Applications. *Adv. Energy Mater.* **6**, 1501793, https://doi.org/10.1002/aenm.201501793 (2016).
4. Dasgupta, N. P. *et al.* 25th Anniversary Article: Semiconductor Nanowires – Synthesis, Characterization, and Applications. *Adv. Mater.* **26**, 2137–2184, https://doi.org/10.1002/adma.201305929 (2014).
5. Wu, R. W. *et al.* Bilayer–metal assisted chemical etching of silicon microwire arrays for photovoltaic applications. *AIP Advances* **6**, 025324, https://doi.org/10.1063/1.4943217 (2016).
6. Lin, H. *et al.* Rational Design of Inverted Nanopencil Arrays for Cost-Effective, Broadband, and Omnidirectional Light Harvesting. *ACS Nano* **8**, 3752–2760, https://doi.org/10.1021/nn500418x (2014).
7. Liang, X. *et al.* Inverted Silicon Nanopencil Array Solar Cells with Enhanced Contact Structures. *Sci. Rep.* **6**, 34139, https://doi.org/10.1038/srep34139 (2016).
8. Lin, H. *et al.* Developing controllable anisotropic wet etching to achieve silicon nanorods, nanopencils and nanocones for efficient photon trapping. *J. Mater. Chem. A* **1**, 9942–9946, https://doi.org/10.1039/c3ta11889d (2013).
9. Vosk, N. A. & Sa'ar, A. Radiative and nonradiative relaxation phenomena in hydrogen- and oxygen-terminated porous silicon. *Nanoscale Research Letters* **9**, 47, https://doi.org/10.1186/1556-276X-9-47 (2014).
10. Um, H. D. *et al.* Versatile control of metal-assisted chemical etching for vertical silicon microwire arrays and their photovoltaic applications. *Sci. Rep.* **5**, 11277, https://doi.org/10.1038/srep11277 (2015).
11. Lai, R. A., Hymel, T. M., Narasimhan, V. K. & Cui, Y. Schottky Barrier Catalysis Mechanism in Metal-Assisted Chemical Etching of Silicon. *ACS Appl. Mater. Interfaces* **8**, 8875–8879, https://doi.org/10.1021/acsami6b01020 (2016).

12. Lianto, P. *et al*. Vertical etching with isolated catalysts in metal-assisted chemical etching of silicon. *Nanoscale* **4**, 7532–7539, https://doi.org/10.1039/c2nr32350h (2012).
13. Lai, C. Q., Zheng, W., Choi, W. K. & Thompson, C. V. Metal assisted anodic etching of silicon. *Nanoscale* **7**, 11123–11134, https://doi.org/10.1039/c5nr01916h (2015).
14. Lee, D. H. *et al*. Strategies for controlling Si nanowire formation during Au-assisted electroless etching. *J. Mater. Chem.* **21**, 10359–10363, https://doi.org/10.1039/c1jm11164g (2011).
15. Kim, J. *et al*. Au/Ag Bilayered Metal Mesh as a Si Etching Catalyst for Controlled Fabrication of Si Nanowires. *ACS Nano* **5**, 3222–3229, https://doi.org/10.1021/nn2003458 (2011).
16. Mikhael, B. *et al*. New Silicon Architectures by Gold-Assisted Chemical Etching. *ACS Appl. Mater. Interfaces* **3**, 3866–3873, https://doi.org/10.1021/am200948p (2011).
17. Wang, D. *et al*. Ordered arrays of nanoporous silicon nanopillars and silicon nanopillars with nanoporous shells. *Nanoscale Research Letters* **8**, 42, https://doi.org/10.1186/1556-276X-8-42 (2013).
18. To, W. K., Tsang, C. H., Li, H. H. & Huang, Z. Fabrication of n-Type Mesoporous Silicon Nanowires by One-Step Etching. *Nano Lett.* **11**, 5252–5258, https://doi.org/10.1021/nl202674t (2011).
19. Hwang, T. Y. *et al*. Morphology control of ordered Si nanowire arrays by nanosphere lithography and metal-assisted chemical etching. *Japanese Journal of Applied Physics* **53**, 05HA07, https://doi.org/10.7567/JJAP.53.05.HA07 (2014).
20. Ratchford, D., Yeom, J. H., Long, J. P. & Pehrsson, P. E. Influence of inhomogeneous porosity on silicon nanowire Raman enhancement and leaky mode modulated photoluminescence. *Nanoscale* **7**, 4124–4133, https://doi.org/10.1039/c4nr06329e (2015).
21. Katiyar, A. K. *et al*. Optical photoresponse of CuS–n-Si radial heterojunction with Si nanocone arrays fabricated by chemical etching. *Phys. Chem. Chem. Phys.* **15**, 20887–20893, https://doi.org/10.1039/c3cp53603c (2013).
22. Cheng, S. L., Lin, H. C., Huang, Y. H. & Yang, S. C. Fabrication of periodic arrays of needle-like Si nanowires on (001)Si and their enhanced field emission characteristics. *RSC Adv.* **7**, 23935–23941, https://doi.org/10.1039/c7ra03733c (2017).
23. Xiu, Y. *et al*. Superhydrophobic and Low Light Reflectivity Silicon Surfaces Fabricated by Hierarchical Etching. *Langmuir* **24**, 10421–10426, https://doi.org/10.1021/la801206m (2008).
24. Li, S. *et al*. Fabrication of porous silicon nanowires by MACE method in HF/H₂O₂/AgNO₃ system at room temperature. *Nanoscale Research Letters* **9**, 196, https://doi.org/10.1186/1556-276X-9-196 (2014).
25. Katiyar, A. K., Sinha, A. K., Manna, S. & Ray, S. K. Fabrication of Si/ZnS Radial Nanowire Heterojunction Arrays for White Light Emitting Devices on Si Substrates. *ACS Appl. Mater. Interfaces* **6**, 15007–150144, https://doi.org/10.1021/ami5028605 (2014).
26. Yang, Q. *et al*. Antireflection effects at nanostructured material interfaces and the suppression of thin-film interference. *Nanotechnology* **24**, 235202, https://doi.org/10.1088/0957-4484/24/23/235202 (2013).
27. Zhang, R. Y. *et al*. Absorption enhancement analysis of crystalline Si thin film solar cells based on broadband antireflection nanocone grating. *J. Appl. Phys.* **110**, 113105, https://doi.org/10.1063/1.3662915 (2011).
28. Zhu, J. *et al*. Optical Absorption Enhancement in Amorphous Silicon Nanowire and Nanocone Arrays. *Nano Lett.* **9**, 279–282, https://doi.org/10.1021/nl802886y (2009).
29. Hwang, I. *et al*. Enhancement of Light Absorption in Photovoltaic Devices using Textured PDMS Stickers. *ACS Appl. Mater. Interfaces* **9**, 21276, https://doi.org/10.1021/acsami.7b04525. (2017).
30. Dawood, M. K. *et al*. Influence of catalytic gold and silver metal nanoparticles on structural, optical, and vibrational properties of silicon nanowires synthesized by metal-assisted chemical etching. *J. Appl. Phys.* **112**, 073509, https://doi.org/10.1063/1.4757009 (2012).
31. Katiyar, A. K. *et al*. Enhancement of Efficiency of a Solar Cell Fabricated on Black Si Made by Inductively Coupled Plasma−Reactive Ion Etching Process: A Case Study of a n-CdS/p-Si Heterojunction Cell. *ACS Appl. Mater. Interfaces* **7**, 23445–23453, https://doi.org/10.1021/acsami.5b04978 (2015).
32. Ray, S. K., Katiyar, A. K. & Raychaudhuri, A. K. One-dimensional Si/Ge nanowires and their heterostructures for multifunctional applications-a review. *Nanotechnology* **28**, 092001, https://doi.org/10.1088/1361-6528/aa565c (2017).
33. Mohammed, M. S. G., Cazzanelli, E., Fasanella, A. & Castriota, M. Silicon Nanocrystals on the Surface of Standard Si Wafers: A Micro-Raman Investigation. *Journal of Materials Science and Chemical Engineering* **6**, 104–116, https://doi.org/10.4236/msce.2018.67012 (2018).
34. Theodorakos, I. *et al*. Picosecond and nanosecond laser annealing and simulation of amorphous silicon thin films for solar cell applications. *J. Appl. Phys.* **115**, 013108, https://doi.org/10.1063/1.4863402 (2014).
35. Balasundaram, K. *et al*. Porosity control in metal-assisted chemical etching of degenerately doped silicon nanowires. *Nanotechnology* **23**, 305304, https://doi.org/10.1088/0957-4484/23/30/305304 (2012).
36. Geyer, N. *et al*. Influence of the doping level on the porosity of silicon nanowires prepared by metal-assisted chemical etching. *Nanotechnology* **26**, 245301, https://doi.org/10.1088/0957-4484/26/24/245301 (2015).
37. Joshi, P. *et al*. 2010 35th IEEE Photovoltaic Specialists Conference (2010).
38. Kai, Q. *et al*. Enhanced light trapping in periodically truncated cone silicon nanowire structure. *J. Semicond.* **36**, 104005, https://doi.org/10.1088/1674-4926/36/10/104005 (2015).
39. Osminkina, L. A. *et al*. Optical properties of silicon nanowire arrays formed by metal-assisted chemical etching: evidences for light localization effect. *Nanoscale Research Letters* **7**, 524. 10.1186/1556-276×−7−524 (2012).
40. Yeom, J. H. *et al*. Decoupling Diameter and Pitch in Silicon Nanowire Arrays Made by Metal-Assisted Chemical Etching. *Adv. Funct. Mater.* **24**, 106–116, https://doi.org/10.1002/adfm.201301094 (2014).
41. Lumerical Solution 8.15, Lumerical Inc. URL https://www.lumerical.com/products/fdtd (2019).
42. Kubota, S. *et al*. FDTD Analysis for Light Passing Through Glass Substrate and Its Application to Organic Photovoltaic with Moth Eye Antireflection Coating. *J. Photopolym. Sci. Technol.* **29**, 209–214, https://doi.org/10.2494/photopolymer.29.209 (2016).
43. Kubota, S. *et al*. Optimized design of moth eye antireflection structure for organic photovoltaics. *J. Coat. Technol. Res.* **13**, 201–210, https://doi.org/10.1007/s11998-015-9745-5 (2016).
44. Palik, E. D. Handbook of Optical Constants of Solids, Academic, Orlando, FL 1985 (1985).

Acknowledgements

Author contributions

Y.J., C.H. and I.Y. designed the project. Y.J., C.H. and Y.H.J. fabricated samples and performed optical and structural characterization studies. Y.J., R.A., H.Y. and I.Y. wrote the manuscript based on discussion with all authors.

Competing interests

The authors declare no competing interests.

Additional information

Supplementary information is available for this paper at https://doi.org/10.1038/s41598-019-52382-4.

Correspondence and requests for materials should be addressed to I.Y.

Reprints and permissions information is available at www.nature.com/reprints.

Publisher's note Springer Nature remains neutral with regard to jurisdictional claims in published maps and institutional affiliations.